

Negative Differential Resistance Induced by Mn Substitution at SrRuO₃/Nb:SrTiO₃ Schottky Interfaces

Yasuyuki Hikita,^{1,*} Lena Fitting Kourkoutis,² Tomofumi Susaki,^{1,†}

David A. Muller,² Hidenori Takagi,¹ and Harold Y. Hwang^{1,3}

¹*Department of Advanced Materials Science,
University of Tokyo, Kashiwa, Chiba 277-8561, Japan*

²*School of Applied and Engineering Physics,
Cornell University, Ithaca, New York 14853, USA*

³*Japan Science and Technology Agency,
Kawaguchi, Saitama 332-0012, Japan*

(Dated: October 31, 2018)

Abstract

We observed a strong modulation in the current-voltage characteristics of SrRuO₃/Nb:SrTiO₃ Schottky junctions by Mn substitution in SrRuO₃, which induces a metal-insulator transition in bulk. The temperature dependence of the junction ideality factor indicates an increased spatial inhomogeneity of the interface potential with substitution. Furthermore, negative differential resistance was observed at low temperatures, indicating the formation of a resonant state by Mn substitution. By spatially varying the position of the Mn dopants across the interface with single unit cell control, we can isolate the origin of this resonant state to the interface SrRuO₃ layer. These results demonstrate a conceptually different approach to controlling interface states by utilizing the highly sensitive response of conducting perovskites to impurities.

PACS numbers: 73.40.Sx, 73.40.Gk, 73.40.-c

I. INTRODUCTION

Schottky junctions using perovskite oxides are systems in which several interesting device properties have been reported, including resistance switching¹, magnetic field sensitive diode², and as a prototypical structure for enhanced photocarrier doping³. One of the important concepts in Schottky junctions is the formation of interface states which strongly influence barrier formation, and in many cases are responsible for nonideal device performance⁴. In elemental metal/conventional semiconductor junctions, interface states are formed as consequences of intrinsic surface reconstructions, impurities or defects on the semiconductor surfaces, or alloying by a metal-semiconductor reaction. In many cases, the barrier formation processes are driven predominantly by the properties of the *semiconductor*, and are usually less dependent on the properties of the metal, with some exceptions such as in the presence of metal-induced-gap states⁵. This is due to the large difference in the bonding character of the constituents, namely spatially oriented covalent bonds in semiconductors and spatially uniform metallic bonds in the metal, which can easily result in amorphous or polycrystalline interfaces.

In contrast, the chemical and structural similarities between metallic and semiconducting perovskites enable the epitaxial growth of oxide heterojunctions. Furthermore, the electrical conductivity in metallic perovskites is often achieved by the delicate energy balance between competing ground states, as seen in high- T_c cuprates or colossal magnetoresistive manganites⁶. Upon doping, many perovskite metals transition through a carrier localized state long before completely becoming an insulator with a well-defined gap in the density of states. When interfaces are formed using such disordered metals, a new type of interface state formation can be anticipated, giving us an additional degree of freedom to manipulate the interface electronic structure from the *metal* side.

To explore these ideas, we have investigated controlled impurity substitution in SrRuO₃/Nb:SrTiO₃ junctions. This is an ideal system to study because the interface is free from a polar discontinuity which can be a significant source of interface states⁷, and its barrier formation is not dominated by interface states, as evidenced by the good agreement between the experimentally determined Schottky barrier height^{8,9} and the Schottky-Mott relation. Additionally, Nb:SrTiO₃ has been the most thoroughly investigated perovskite semiconductor in junction structures, such as the Schottky barrier height characterization⁸

and the studies of non-linear dielectric constant and its effect on band bending^{10,11}. SrRuO₃, in the absence of chemical substitution, is a representative conducting perovskite, with a ferromagnetic transition temperature $T_C = 160$ K. It exhibits several unusual transport properties, such as the absence of resistivity saturation up to 1000 K¹². The strong divergence of dR/dT as $T \rightarrow T_C^+$ and the weak divergence when $T \rightarrow T_C^-$ raises questions of the applicability of the standard Boltzmann transport picture, leading to the assignment of SrRuO₃ as a "bad metal"¹³. As can be expected from the unusual behavior in its pure form, SrRuO₃ is highly sensitive to disorder induced by chemical doping such as Ca¹⁴, Zn, Ni, Co¹⁵, Fe¹⁶ or Mn^{15,17,18} doping, all of which induce metal-insulator transitions. In the case of doping with a 3d transition metal ion at the Ru site, the Ru-O bonding network is reduced and carrier localization occurs because of the localized nature of the 3d orbitals.

Here, we study the effects of using a strongly correlated metal at the junction interface by examining the temperature dependent I - V characteristics of Mn-doped SrRuO₃/Nb:SrTiO₃ Schottky junctions. From the high temperature slope in the semi-logarithmic plot of the I - V characteristics, the spatial distribution of the barrier height increased by Mn substitution. At low temperatures, we observed negative differential resistance even for a single layer of Mn substituted SrRuO₃ metal at the interface. These results indicate that the high sensitivity of strongly correlated metals to impurities can give rise to characteristic interface state formation from imperfectly screened impurity ions.

II. EXPERIMENTAL

Epitaxial thin film structures were fabricated by pulsed laser deposition using a KrF excimer laser with a fluence of 2.0 J/cm² on SrTiO₃(100) substrates undoped and Nb = 0.5 wt % doped in an oxygen partial pressure (P_{O_2}) of 0.3 Torr (unless otherwise indicated) and at a substrate temperature of 800 °C. The deposited film thickness of SrRuO₃ and SrRu_{0.95}Mn_{0.05}O₃ were 800 Å. Polycrystalline SrRu_{1-x}Mn_xO₃ ($x = 0, 0.05, 0.15$), SrMnO₃, SrTi_{0.95}Mn_{0.05}O₃ and single crystal SrTiO₃ targets were used.

The critical concentration required for the bulk metal-insulator transition in SrRu_{1-x}Mn_xO₃ is $x = 0.4$ (Ref. 18). At $x = 0.05$, predominantly studied here, SrRu_{1-x}Mn_xO₃ is reported to be a metal with a slightly increased resistivity and a reduced T_C . The X-ray diffraction patterns of the thin films revealed high quality epitaxial

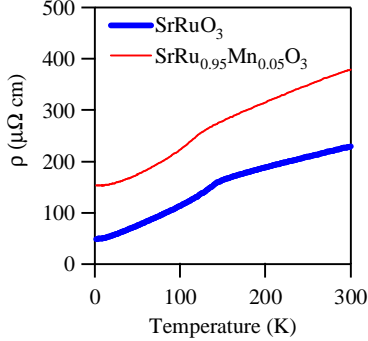


FIG. 1: (Color online) Temperature dependent resistivity (ρ) of the SrRuO₃ (bold) and SrRu_{0.95}Mn_{0.05}O₃ (solid) thin films grown on SrTiO₃(100) substrates. The increased resistivity and the reduced T_C is evident for the SrRu_{0.95}Mn_{0.05}O₃ thin film.

growth and an out-of-plane lattice constant of 3.95 Å for both SrRu_{0.95}Mn_{0.05}O₃ and undoped SrRuO₃. As shown in Fig. 1, the temperature dependent resistivity (ρ) of the films deposited on insulating SrTiO₃(100) substrates exhibited metallic behavior with a T_C and residual resistivity of 150 K and 50 $\mu\Omega$ cm for SrRuO₃, and 140 K and 150 $\mu\Omega$ cm for SrRu_{0.95}Mn_{0.05}O₃.

III. RESULTS

A. Temperature dependent I - V characteristics

The temperature dependent I - V characteristics for SrRuO₃/Nb:SrTiO₃ and SrRu_{0.95}Mn_{0.05}O₃/Nb:SrTiO₃ are shown in Fig. 2(a) and (b), respectively. Ohmic contacts were made by Ag paste directly on the ruthenates and Al deposition on Nb:SrTiO₃. The polarity of the applied bias is defined as positive voltage applied to the ruthenate.

In the case of the SrRuO₃ junction, the forward bias current in the semi-logarithmic plot is linearly proportional to the bias voltage with an overall shift to higher voltages at lower temperatures, indicating near ideal Schottky behavior. The current transport mechanism of these junctions was determined from the Richardson plot shown in Fig. 3(a). The reduced slope at high temperatures indicates the contribution of thermoionic field emission (TFE), which is consistent with the large reverse bias current caused by the high

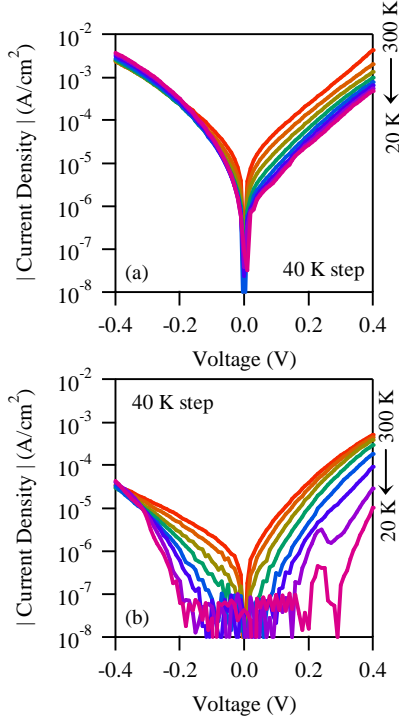


FIG. 2: (Color online) Temperature dependence of the I - V characteristics in (a) $\text{SrRuO}_3/\text{Nb:SrTiO}_3$ and (b) $\text{SrRu}_{0.95}\text{Mn}_{0.05}\text{O}_3/\text{Nb:SrTiO}_3$ junctions. Measurements taken between 300 K and 20 K in 40 K steps.

doping concentration in Nb:SrTiO_3 . The gradual increase in J_S/T^2 at low temperatures corresponds to the dominance of the field emission (FE) process in this temperature regime. Here, J_S is the saturation current density obtained by a linear extrapolation of the forward biased region of the I - V characteristics to zero voltage. The temperature dependence of the two junctions is very similar to what has been observed in $\text{Au}/\text{Nb:SrTiO}_3$ Schottky junctions^{11,19}.

In contrast, two apparent differences can be seen in the I - V characteristics of the $\text{SrRu}_{0.95}\text{Mn}_{0.05}\text{O}_3/\text{Nb:SrTiO}_3$ junction, compared to the $\text{SrRuO}_3/\text{Nb:SrTiO}_3$ junction (Fig. 2). First, the large decrease in the current over the measured voltage range by almost an order of magnitude, and second, the appearance of current peaks and negative differential resistance (NDR) at forward bias below 60 K. Since the NDR behavior is observed in the FE low temperature region, Mn substitution appears to induce a resonant state similar to a double barrier resonant tunneling diode²⁰. A linear plot of the magnified I - V

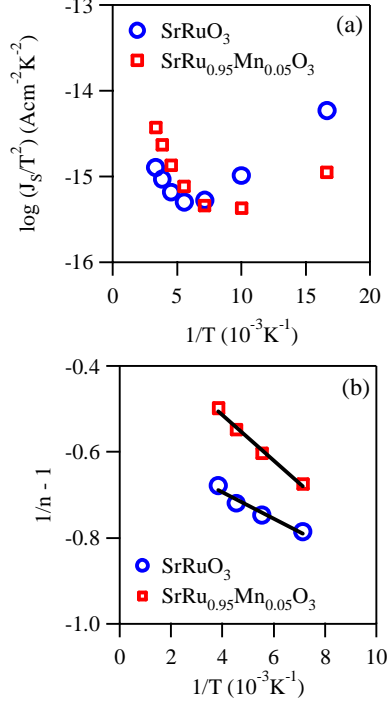


FIG. 3: (Color online) (a) Richardson plot of SrRuO_3 ($\text{SrRu}_{0.95}\text{Mn}_{0.05}\text{O}_3$)/ Nb:SrTiO_3 junctions showing a crossover from thermoionic field emission to field emission. (b) Evaluation of the Schottky barrier height spatial inhomogeneity from the ideality factors. The circles (squares) denote SrRuO_3 ($\text{SrRu}_{0.95}\text{Mn}_{0.05}\text{O}_3$) and the lines are linear fits to the experimental data in the high temperature regime.

characteristics and the normalized conductance for $\text{SrRu}_{0.95}\text{Mn}_{0.05}\text{O}_3$ is shown in Fig. 4(a) and (b), respectively. As the temperature is decreased, a current peak emerges at $\sim +0.25$ V. Measurements taken under an applied magnetic field of 13 T revealed no significant difference in either the peak voltage or the conductance, indicating that this is a charge state, not a collective magnetic state.

The large decrease in the current can be quantitatively addressed by analyzing the temperature dependence of the junction ideality factor which indicates the degree of spatial inhomogeneity of the Schottky barrier heights $(\Phi_{SB})^{21}$. The assumptions of a Gaussian distribution and voltage dependence of the Φ_{SB} give the following relationship, which agrees with many experimental results²¹:

$$\frac{1}{n(T)} - 1 = \rho_2 + \frac{\rho_3}{2kT/q}. \quad (1)$$

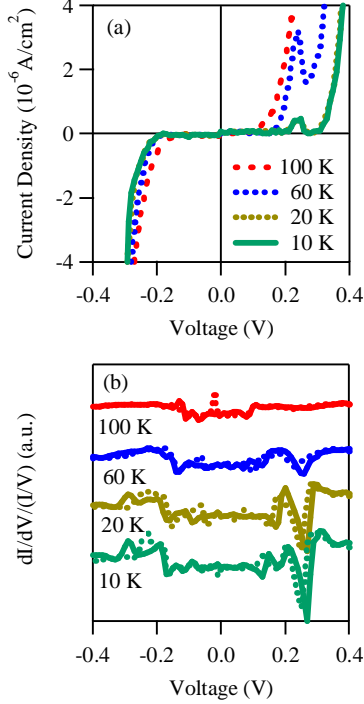


FIG. 4: (Color online) Temperature dependence of the (a) I - V characteristics and (b) the normalized conductance in a $\text{SrRu}_{0.95}\text{Mn}_{0.05}\text{O}_3/\text{SrTiO}_3$ junction. Solid (dotted) lines in (b) denote a voltage sweeps in the positive (negative) direction. NDR emerges as the temperature is decreased.

Here, n is the ideality factor, k the Boltzmann constant, and q the electronic charge. ρ_2 is a measure of the sensitivity of Φ_{SB} to the applied voltage and ρ_3 corresponds to the standard deviation in Φ_{SB} . The present results plotted following Eq. (1) are shown in Fig. 3(b). The obtained values (ρ_2, ρ_3) are $(-0.57, 5.31 \text{ meV})$ for SrRuO_3 and $(-0.30, 9.08 \text{ meV})$ for $\text{SrRu}_{0.95}\text{Mn}_{0.05}\text{O}_3$. The increase in ρ_3 by almost a factor of two for the Mn-doped junction indicates that the presence of Mn ions increases potential fluctuations at the interface.

B. Interface modulation

To verify the role of Mn doping on the NDR, we fabricated modulated heterointerfaces where the Mn concentration was varied across the interface as shown in Fig. 5(a). In the five structures, the location of the Mn ions is systematically varied with respect to the interface. Structures with single unit cell (uc) features were deposited while monitoring the reflection high-energy electron diffraction (RHEED) intensity. A two stage differential pumping setup

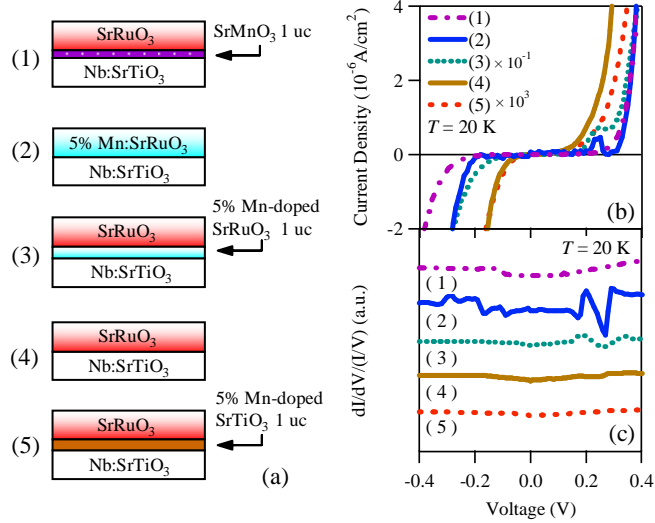


FIG. 5: (Color online) (a) Schematic diagram of the artificial structures grown to systematically vary the distribution of Mn ions with respect to the interface. (1) $\text{SrRuO}_3/[\text{SrMnO}_3]_{1\text{uc}}/\text{Nb:SrTiO}_3$, (2) $\text{SrRu}_{0.95}\text{Mn}_{0.05}\text{O}_3/\text{Nb:SrTiO}_3$, (3) $\text{SrRuO}_3/[\text{SrRu}_{0.95}\text{Mn}_{0.05}\text{O}_3]_{1\text{uc}}/\text{Nb:SrTiO}_3$, (4) $\text{SrRuO}_3/\text{Nb:SrTiO}_3$, (5) $\text{SrRuO}_3/[\text{SrTi}_{0.95}\text{Mn}_{0.05}\text{O}_3]_{1\text{uc}}/\text{Nb:SrTiO}_3$. (b) I - V characteristics and (c) the normalized conductance of the structures illustrated in (a). NDR is observed only in structures (2) and (3).

enabled RHEED observations at high pressure.

In structure (1), one unit cell of SrMnO_3 is deposited on the Nb:SrTiO_3 substrate at $P_{\text{O}_2} = 0.1$ Torr, followed by a thick layer of SrRuO_3 . The reduced current density in the whole voltage range at 20 K can be attributed to the high resistivity of SrMnO_3 at low temperatures, and as is evident from Fig. 5(b), no NDR was observed. In structure (2) the surface of the Nb:SrTiO_3 is fully covered with $\text{SrRu}_{0.95}\text{Mn}_{0.05}\text{O}_3$ as discussed above. In structure (3), one unit cell of $\text{SrRu}_{0.95}\text{Mn}_{0.05}\text{O}_3$, grown at $P_{\text{O}_2} = 0.1$ Torr, is inserted between a thick layer of SrRuO_3 and the Nb:SrTiO_3 substrate. The basic features of the I - V characteristics are the same as in $\text{SrRuO}_3/\text{Nb:SrTiO}_3$ but with the presence of a current peak, implying that the origin of the observed NDR is not caused by the modification of the band alignment but the modification of the local interface structure. Structure (4) is the case of $\text{SrRuO}_3/\text{Nb:SrTiO}_3$, which is shown again for comparison. The extreme case, simulating a situation where the Mn ions are embedded inside Nb:SrTiO_3 , is demonstrated in structure (5). Here, a single unit cell of $\text{SrTi}_{0.95}\text{Mn}_{0.05}\text{O}_3$ was deposited on Nb:SrTiO_3

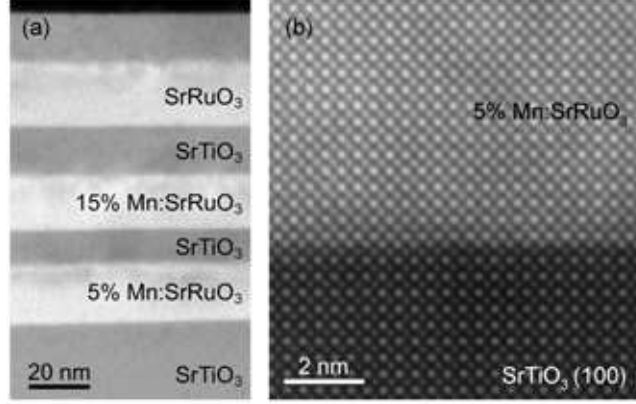


FIG. 6: Annular dark field STEM images of a $(\text{SrRu}_{1-x}\text{Mn}_x\text{O}_3/\text{SrTiO}_3)$ multilayer. (a) Overview of the structure. (b) High magnification image of the abrupt $\text{SrRu}_{0.95}\text{Mn}_{0.05}\text{O}_3/\text{SrTiO}_3$ interface.

at $P_{\text{O}_2} = 1.0 \times 10^{-5}$ Torr, followed by the deposition of SrRuO_3 . From investigations of the leakage current at metal/Mn-doped SrTiO_3 contacts, Mn-doped SrTiO_3 is known to be insulating^{22,23}. In this case also no NDR was observed.

The above investigation has given evidence that the appearance of the low temperature NDR is associated with the presence of a low concentration of Mn ions on the metal side, ruling out the possibility of Mn, embedded in the substrate by diffusion or implantation acting as ionic potentials within the depletion region^{24,25}. The absence of the current peak in structure (1) is ascribed to the formation of a SrMnO_3 *band* rather than isolated atomic states at the interface.

C. Electron microscopy and spectroscopy

The microscopic structure of the ruthenate/titanate interface was analyzed using scanning transmission electron microscopy (STEM) performed in a 200 kV FEI Tecnai F20 STEM. A superlattice of SrRuO_3 (20 nm)/ SrTiO_3 (10 nm)/ $\text{SrRu}_{0.85}\text{Mn}_{0.15}\text{O}_3$ (20 nm)/ SrTiO_3 (10 nm)/ $\text{SrRu}_{0.95}\text{Mn}_{0.05}\text{O}_3$ (20 nm) was fabricated on a $\text{SrTiO}_3(100)$ substrate (Fig. 6(a)). An annular dark field (ADF) STEM image of the interface between the substrate and the first ruthenate layer, $\text{SrRu}_{0.95}\text{Mn}_{0.05}\text{O}_3$, is shown in Fig. 6(b), demonstrating that the interface is chemically abrupt, with no obvious defects or dislocations. All Schottky junctions analyzed in this work were prepared under similar conditions as the test structure above,

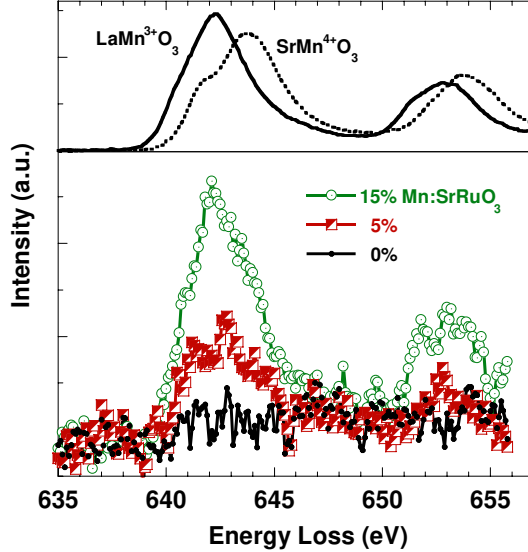


FIG. 7: (Color online) Mn- $L_{2,3}$ electron energy loss spectra from the three Mn doped SrRuO_3 layers imaged in Fig. 6(a). For comparison Mn^{3+} and Mn^{4+} reference spectra are shown.

suggesting that the interfaces in these junctions are of comparable quality. In order to understand the local bonding of the Mn dopants in $\text{SrRu}_{1-x}\text{Mn}_x\text{O}_3$, electron energy loss spectroscopy (EELS) was performed. From the simple picture of Mn for Ru substitution in $\text{SrRu}_{0.95}\text{Mn}_{0.05}\text{O}_3$, a Mn valence state of 4+ is expected, however, Mn^{3+} can also be present due to charge disproportionation in the form of $\text{Mn}^{4+} + \text{Ru}^{4+} \rightleftharpoons \text{Mn}^{3+} + \text{Ru}^{5+}$ (Ref. 26). In Fig. 7, the Mn- $L_{2,3}$ spectra for the three ruthenate layers are compared to Mn^{3+} and Mn^{4+} reference spectra obtained from bulk LaMnO_3 and SrMnO_3 , respectively²⁷. From the peak position of the Mn- L_3 edge a Mn valence of 3 ± 0.3 in the Mn doped ruthenate layers can be inferred.

IV. DISCUSSION

From the above studies, we have found that impurity doping on the metal side can strongly influence the electronic structure at the interface. We consider the relation between Mn doping in SrRuO_3 and the NDR by examining the electronic structures of the two parent compounds SrRuO_3 and SrMnO_3 . In SrRuO_3 , the crystal field splitting $10Dq$ of ~ 3 eV is obtained from optical spectroscopy measurements²⁸, and the oxygen $2p$ band lies below the

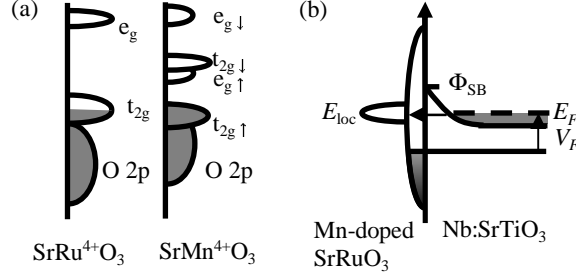


FIG. 8: (a) A schematic diagram of the density of states for SrRuO₃ and SrMnO₃. (b) Interface band diagram illustrating the localized state on the metal side of the interface. V_F is the applied forward bias voltage, E_F is the Fermi level, Φ_{SB} the Schottky barrier height, and E_{loc} is the localized state at the interface.

Ru t_{2g} band where the Fermi level is located as shown in Fig. 8(a). We base our discussion on SrMnO₃ with a cubic G-type antiferromagnetic ground state for which the theoretically calculated density of states are schematically shown in Fig. 8(a). The top of the valence band overlaps with the oxygen 2p band and the Mn e_g bands are located ~ 0.3 eV above the Fermi level²⁹. Within a rigid band picture, the Ru to Mn substitution modifies the empty states of SrRuO₃ arising from the Mn e_g states. Furthermore, the doping independent lattice constant favors Mn ions to be localized owing to their smaller cation radius.

The observation of the current peak at *forward* bias and below 1.47 eV, the Φ_{SB} of SrRuO₃/Nb:SrTiO₃(100)⁸, further support the above band structure consideration. Only when the localized states (E_{loc}) lie between the Fermi level (E_F) and Φ_{SB} , can NDR be observed under *forward* bias, as illustrated in Fig. 8(b). In other cases, either the current will be dominated by the large FE current, or the localized states are buried in the large density of states of the host. We conclude that the NDR observed at the SrRu_{0.95}Mn_{0.05}O₃/Nb:SrTiO₃ interface is caused by the localized Mn e_g states inside SrRu_{0.95}Mn_{0.05}O₃ acting as the resonant state.

V. CONCLUSIONS

We have applied the highly sensitive response of metallic perovskites to impurities in a Schottky junction to demonstrate that the interface electronic structure can be strongly modified by introduction of substitutional impurities on the *metal* side. The change in the

junction characteristics induced by impurity doping is unexpectedly large considering the small differences in the in-plane bulk transport properties. In addition to the enhanced spatial fluctuation of the interface potential, the dispersed Mn ions act as resonant states giving rise to NDR in the I - V characteristics. The poor electrostatic screening generally present in metallic perovskites and the close similarity in the chemical bonding between metallic and semiconducting perovskites can result in robust interface states exhibiting the character of the impurity element. Further studies may lead to designing resonant tunneling structures by simple doping of a metallic host, or as a prototypical structure for spectroscopic investigation of screening, localization, and metal-insulator transitions in strongly correlated electron systems.

Acknowledgments

This work was supported by the TEPCO Research Foundation and a Grant-in-Aid for Scientific Research on Priority Areas. Y.H. acknowledges support from the Grant-in-Aid 21st Century COE Program at the University of Tokyo. The work at Cornell University was supported under the ONR EMMA MURI monitored by Colin Wood. L. F. K. acknowledges financial support by Applied Materials.

-
- * Electronic address: hikita@k.u-tokyo.ac.jp
- † Present address: Materials and Structures Laboratory, Tokyo Institute of Technology, Yokohama, Kanagawa 226-8503, Japan.
- ¹ A. Beck, J. G. Bednorz, C. Gerber, C. Rossel, and D. Widmer, *Appl. Phys. Lett.* **77**, 139 (2000).
- ² N. Nakagawa, M. Asai, Y. Mukunoki, T. Susaki, and H. Y. Hwang, *Appl. Phys. Lett.* **86**, 082504 (2005).
- ³ H. Katsu, H. Tanaka, and T. Kawai, *Appl. Phys. Lett.* **76**, 3245 (2000).
- ⁴ E. H. Rhoderick and R. H. Williams, *Metal-Semiconductor Contacts* (Clarendon, Oxford, 1988).
- ⁵ V. Heine, *Phys. Rev.* **138A**, 1689 (1965).
- ⁶ M. Imada, A. Fujimori, and Y. Tokura, *Rev. Mod. Phys.* **70**, 1039 (1998).
- ⁷ N. Nakagawa, H. Y. Hwang, and D. A. Muller, *Nature Mater.* **5**, 204 (2006).
- ⁸ Y. Hikita, Y. Kozuka, T. Susaki, H. Takagi, and H. Y. Hwang, *Appl. Phys. Lett.* **90**, 143507 (2007).
- ⁹ M. Minohara, I. Ohkubo, H. Kumigashira, and M. Oshima, *Appl. Phys. Lett.* **90**, 132123 (2007).
- ¹⁰ T. Yamamoto, S. Suzuki, K. Kawaguchi, and K. Takahashi, *Jpn. J. Appl. Phys.* **37**, 4737 (1998).
- ¹¹ T. Susaki, Y. Kozuka, Y. Tateyama, and H. Y. Hwang, *Phys. Rev. B* **76**, 155110 (2007).
- ¹² P. B. Allen, H. Berger, O. Chauvet, L. Forro, T. Jarlborg, A. Junod, B. Revaz, and G. Santi, *Phys. Rev. B* **53**, 4393 (1996).
- ¹³ L. Klein, J. S. Dodge, C. H. Ahn, G. J. Snyder, T. H. Geballe, M. R. Beasley, and A. Kapitulnik, *Phys. Rev. Lett.* **77**, 2774 (1996).
- ¹⁴ F. Fukunaga and N. Tsuda, *J. Phys. Soc. Japan* **63**, 3798 (1994).
- ¹⁵ L. Pi, A. Maignan, R. Retoux, and B. Raveau, *J. Phys: Condens. Matter* **14**, 7391 (2002).
- ¹⁶ C. Bansal, H. Kawanaka, R. Takahashi, and Y. Nishihara, *J. Alloys. Comp.* **360**, 47 (2003).
- ¹⁷ G. N. Banerjee, R. N. Bhowmik, and R. Ranganathan, *J. Phys: Condens. Matter* **13**, 9481 (2001).
- ¹⁸ G. Cao, S. Chikara, X. N. Lin, E. Elhami, V. Durairaj, and P. Schlottmann, *Phys. Rev. B* **71**, 035104 (2005).
- ¹⁹ H. Hasegawa and T. Nishino, *J. Appl. Phys.* **69**, 1501 (1991).
- ²⁰ R. Tsu and L. Esaki, *Appl. Phys. Lett.* **22**, 562 (1973).

- ²¹ J. H. Werner and H. H. Guttler, *J. Appl. Phys.* **69**, 1522 (1990).
- ²² W. Hofman, S. Hoffmann, and R. Waser, *Thin Solid Films* **305**, 66 (1997).
- ²³ K. Morito, T. Suzuki, and M. Fujimoto, *Jpn. J. Appl. Phys.* **40**, 5493 (2001).
- ²⁴ S. Modesti, D. Furlanetto, M. Piccin, S. Rubini, and A. Franciosi, *Appl. Phys. Lett.* **82**, 1932 (2003).
- ²⁵ J. Caro, I. D. Vink, G. D. J. Smit, S. Rogge, T. M. Klapwijk, R. Loo, and M. Caymax, *Phys. Rev. B* **69**, 125324 (2004).
- ²⁶ R. K. Sahu, Z. Hu, M. L. Rao, S. S. Manoharan, T. Schmidt, B. Richter, M. Knupfer, M. Golden, J. Fink, and C. M. Schneider, *Phys. Rev. B* **66**, 144415 (2002).
- ²⁷ LaMnO₃ bulk specimen was supplied by Toshima Manufacturing Co., Ltd. SrMnO₃ specimen was prepared by sintering SrCO₃ and MnO₂ in molar ratio at 1300 °C for 24 hours repeatedly with interval grinding.
- ²⁸ Y. S. Lee, J. S. Lee, T. W. Noh, D. Y. Byun, K. S. Yoo, K. Yamaura, and E. Takayama-Muromachi, *Phys. Rev. B* **67**, 113101 (2003).
- ²⁹ R. Sondena, P. Ravindran, S. Stolen, T. Grande, and M. Hanfland, *Phys. Rev. B* **74**, 144102 (2006).